International Journal of Emerging Technology and Advanced Engineering
Website: www.ijetae.com (ISSN 2250-2459, ISO 9001:2008 Certified Journal, Volume 4, Issue 1, January 2014)

Terahertz Imaging for Nondestructive Evaluation of Packaged Power Electronic Devices

Nathan M. Burford[1], Magda O. El-Shenawee[2], Chad B. O'Neal[3], Kraig J. Olejniczak[4]

[1]*Microelectronics-Photonics Program, University of Arkansas, Fayetteville, AR 72701 USA*
[2] *Department of Electrical Engineering, University of Arkansas, Fayetteville, AR 72701 USA*
[3,4]*Arkansas Power Electronics International, Inc., Fayetteville, AR 72701 USA*

***Abstract*— Terahertz (THz) time-domain imaging of power electronic devices is performed using the commercial TPSTM Spectra 3000 THz imaging and spectroscopy system. The dimensions of bond wires within power transistor packages are extracted and the time-of-flight tomography is used to illustrate depth profiling of features in the device package. The devices under test in this paper are plastic encapsulated. The encapsulation measures a few millimeters thick. The THz images obtained in the reflection mode demonstrate a potential tool for the non-destructive inspection of packaged power electronic devices.**

***Keywords*— Image processing, nondestructive testing, power transistors, quality control, terahertz (THz).**

I. Introduction

Nondestructive inspection and evaluation of packaged electronic devices is of significant interest to the power electronics industry [1-3]. Failure analysis, quality control and even reverse engineering all require imaging through optically opaque layers that may not be easily removed for visual inspection. Terahertz Time-Domain Spectroscopy (THz-TDS) imaging offers promising potential for truly non-contact, nondestructive visualization of features in such packaged power electronics. The THz band was historically defined to lie between approximately 0.1 and 10 THz due to the longstanding difficulties with efficiently generating and measuring radiation at these frequencies [3]. Recent advances in improving efficiency and stability of THz sources, while reducing the cost of this technology, has made imaging and spectroscopy in the THz band much more practical. However, few companies are now manufacturing commercial THz imaging and spectroscopy systems.

Conventional inspection methods used for packaged devices include x-ray transmission imaging [4] and scanning acoustic microscopy (SAM) [5]. X-ray transmission imaging utilizes high energy photons that can potentially ionize atoms in a semiconductor, permanently damaging and altering electrical properties of the material.

SAM imaging, on the other hand, requires samples to be immersed in a liquid medium, often water. This has the potential for water contamination of packaged components, which can lead to oxidation and degradation of the device performance.

On the other hand, the THz-TDS imaging offers several potential improvements over these traditionally implemented imaging methods. Unlike high energy x-ray photons, THz band photon energies are well below damaging ionization energies [3]. The shorter wavelength of THz waves as compared to millimeter waves provides higher spatial resolution while still providing adequate penetration into dielectric materials. Also, THz imaging does not require immersion of samples in liquids, eliminating the risk of oxidation damage from water inherent with SAM imaging [3].

Several previous works have investigated the use of the THz spectrum for nondestructive inspection and characterization of electronic devices. The earliest demonstration of imaging packaged electronics with THz waves to our knowledge was performed in 1995 by Hu and Nuss [6]. In this work, THz time-domain transmission imaging was performed on a semiconductor integrated circuit, revealing metal interconnects through an optically opaque plastic housing. Yamashita et al. presented a non-contact method using a laser terahertz emission microscope for detecting failures in individual p-n junctions in integrated circuits. Exciting individual junctions with focused ultrafast optical laser pulses caused the emission of THz pulses from the junctions. A correlation between the THz waveforms of normal junctions compared to defective ones was conducted [7, 8]. Another method was developed by Huber et al. for subwavelength confining of THz radiation, allowing for the visualization of mobile carriers in semiconductor nanodevices with spatial resolutions of approximately 40 nm [9]. Additionally, Nakanishi et al. utilized THz-TDS to successfully measure via depth in silicon wafers, confirming observed experimental results with Finite-Difference Time-Domain simulations [10].

International Journal of Emerging Technology and Advanced Engineering
Website: www.ijetae.com (ISSN 2250-2459, ISO 9001:2008 Certified Journal, Volume 4, Issue 1, January 2014)

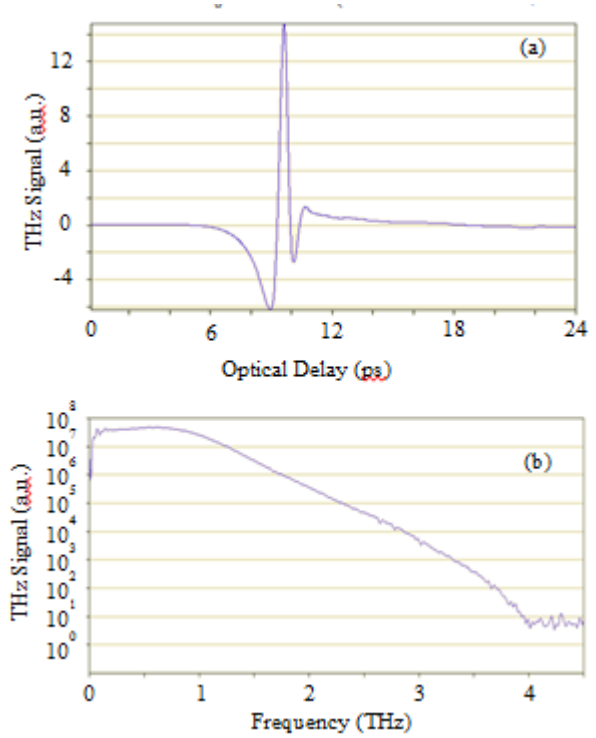

Fig. 1. (a) Reference time-domain pulse and (b) frequency domain of the Terahertz Time-Domain Spectroscopy (THz-TDS) system.

The THz-TDS was also used by Minkevicius et al. in conjunction with unique data processing methods to image soldered tab wires on silicon solar panels leading to successful location of soldering defects [11].

This paper presents the results from an investigation of THz-TDS imaging for various applications in power electronic device inspection. Silicon carbide (SiC) power transistors and half-bridge modules, and high temperature Si solar cells were investigated. In this work, reflection imaging is of interest. Section II describes the THz-TDS system in reflection mode. The imaging results for extracting useful information from the SiC power transistors will be presented in Section III, with a brief discussion of results from the other samples. All samples used in this work were provided by Arkansas Power Electronics International, Inc. (APEI, Inc.) to investigate the potential use of THz imaging and spectroscopy techniques for failure analysis of packaged devices.

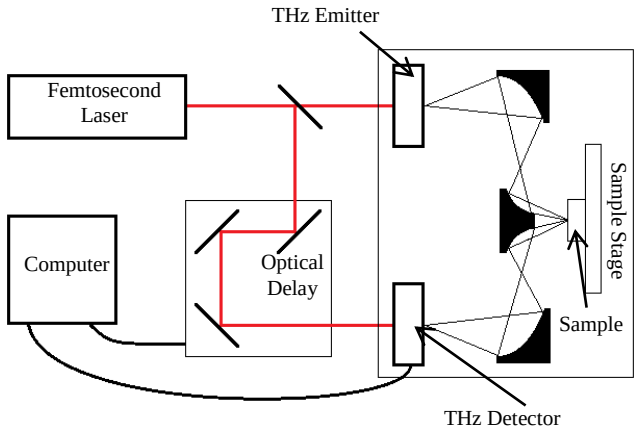

Fig. 2. Schematic of the Terahertz Time-Domain Spectroscopy (THz-TDS) reflection imaging system.

II. Methodology

A. *THz-TDS System Overview*

Imaging with THz TDS of various packaged electronic device samples was performed utilizing a TPS™ Spectra 3000 spectrometer (Teraview Limited, Cambridge, UK). This THz pulsed spectroscopy system had a spectral range of 0.06 to 4 THz. The reference THz pulse taken in transmission mode is shown in Fig. 1(a). Taking the Fourier transform of this pulse gives the frequency response, shown in Fig. 1(b). A schematic of the reflection imaging module of the system is illustrated in Fig. 2. Here, a mode-locked Ti:sapphire laser (Menlo Systems, Martinsried, Germany) with a free-space wavelength of 800 nm, sub-100 femtosecond pulse duration, 80 MHz repetition rate and 300 mW average maximum power excites photocarriers in the gallium arsenide (GaAs) THz emitter. A DC voltage bias is placed across the dipole antenna of the emitter, which forces the excited photo-generated carriers to be collected by the antenna, thus emitting a THz pulse. Similar methods for generating THz pulses are described in detail in [12] and [13].

THz imaging in this work is accomplished utilizing similar GaAs antennas [12, 13]. The THz pulse, after being reflected off or transmitted through the sample, induces a measurable current in the receiving antenna that is proportional to the intensity of the THz field.

International Journal of Emerging Technology and Advanced Engineering
Website: www.ijetae.com (ISSN 2250-2459, ISO 9001:2008 Certified Journal, Volume 4, Issue 1, January 2014)

The same Ti:sapphire laser is used to gate the antenna. By sweeping the delay length of the optical laser pulse, a current proportional to the received THz field is induced across the antenna and can be measured at discrete points in time. This allows the full THz waveform – amplitude and phase – to be measured.

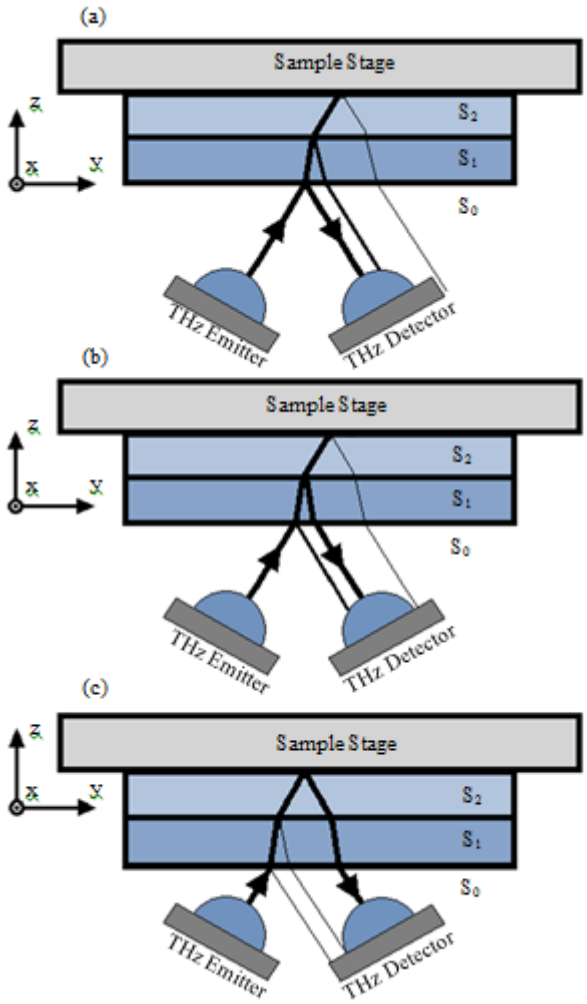

Fig. 3. Cross section illustration of a multilayered sample mounted on the RIM. Sample position in the *z*-direction is adjusted to align the THz detector with the (a) reflection from S_0, (b) reflection from S_1 and (c) reflection from S_2.

On both the emitter and receiver, the THz pulse is focused using hemispherical silicon lenses. Gold surfaced parabolic mirrors focus the THz radiation onto the sample. The reflection imaging module (RIM) allows samples to be systematically scanned across the THz beam, thus acquiring reflectance spectra for each pixel of the image. This image is referred to as the c-scan.

Threaded shaft stepper motors allow a two-dimensional scan area of up to 2 cm × 2 cm, with step sizes down to 50 μm. A compartment of size 20 cm × 12 cm × 10 cm, where the samples are located, is purged by using compressed nitrogen gas to eliminate water vapor. As known, water has strong absorption spectra in the THz band, which can greatly increase the noise and hence degrade the quality of the image.

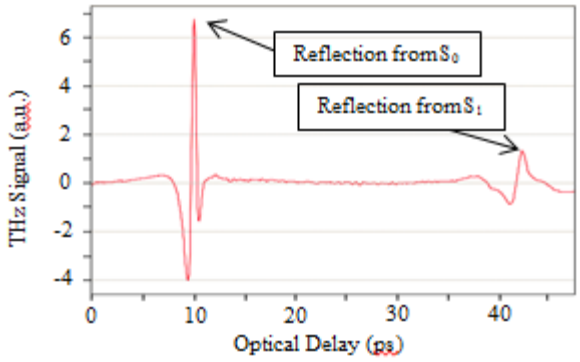

Fig. 4. Reflected THz pulses from a multilayered SiC transistor.

In other words, this purging removes water molecules from the THz beam path without requiring vacuum pumping, allowing the samples to be kept at atmospheric pressure.

In addition to two-dimensional (2D) scanning across the x-y plane, the distance z from the sample surface to the THz beam focal point can be manually adjusted. This not only allows the THz beam to be focused on the sample surface, but also allows for improved imaging of buried layers (i.e. multilayers as shown in Fig. 3). Consider the cross section view of a multilayered sample illustrated in Fig. 3(a). As shown, the sample is positioned on the z-axis such that the focal point of the THz beam lies on the top surface of the sample, S_0. This aligns the reflection from S_0 with the THz receiver optics, however, reflections from S_1 and S_2 are not aligned and therefor the measured amplitudes of the reflections from these layers are observed to be lower than their maximum values. When the sample stage is moved in the negative z-direction as shown in Figs. 3(b) and 3(c) the THz receiver optics can be aligned with reflections from S_1 and S_2, respectively. The time-domain signal from a SiC transistor is shown in Fig. 4. Transistors have a multilayered structure similar to that illustrated in Fig. 3. In Fig. 4 multiple reflections are seen; a strong reflection from the top surface S_0 located at approximately 10 ps and a lower amplitude reflection from the first buried surface S_1 is located around 42 ps.

International Journal of Emerging Technology and Advanced Engineering
Website: www.ijetae.com (ISSN 2250-2459, ISO 9001:2008 Certified Journal, Volume 4, Issue 1, January 2014)

Focusing the beam on either of these surfaces will maximize the amplitude in the pulse reflection from that surface, while reducing the amplitude of other reflections. This process is observed to improve the quality of reflection images of the buried layers in the sample as compared to imaging with the beam focused on the top surface only.

B. Time-of-Flight Depth Profiling

Depth profiling of features immersed in a homogenous medium can be performed utilizing time-of-flight tomography [1]. The height/depth can be shown to be

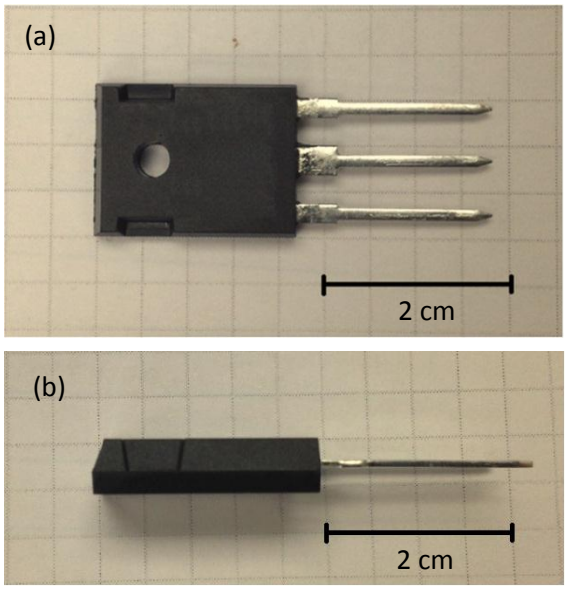

Fig. 5. Top (a) and side (b) views of a SiC transistor (Transistor 1).

$$\Delta h = \Delta t \cdot c \cdot \cos\theta_r/(2 \cdot n) - \Delta d \cdot \cos\theta_r/(n \cdot \cos\theta_i) \quad (1)$$

Where Δh is the height/depth of the feature of interest with respect to the reference surface, c is the speed of light in vacuum, n is the refractive index of the surrounding medium, θ_i and θ_r are the angles of incidence and refraction of the incident beam, respectively, Δd is physical displacement of the THz emitter/receiver when the beam focus is moved from the feature surface to the reference surface, and Δt is the time delay difference between the pulse reflection off the feature surface and reference surface.

C. Image Processing

Image resolution is limited by the spot size of the THz beam as well as the diffraction limit. Both of these are dependent on the individual frequency components of the broadband THz pulse, with lower and higher frequencies contributing to lower and higher resolution, respectively. As seen in the Fourier transform of the time-domain pulse illustrated in Fig. 1(b), the bandwidth of the pulse is approximately 0.08 to 4 THz, with frequencies above 1 THz steadily decreasing in power.

Pulsed time-domain imaging returns the full time-dependent THz signal at each x-y location. As such, there are many ways to interpret the data in order to generate an image. Some examples include time slicing, where the power of the time-domain signal at a single, constant point in time is returned for each pixel; peak amplitude, which involves locating the maximum value of the time-domain signal and returning either that maximum value or the time location of the peak for each pixel; signal integration, where the time-domain signal is integrated between two constant points in time and the value of this integral is returned at each pixel.

In order to improve the resolution of time-domain images, frequency-domain filtering is implemented in order to remove low resolution, low frequency components of the signal. At each pixel, the Fourier transform of the time-domain signal is taken. Once in the frequency domain, a Gaussian high-pass filter,

$$1 - e^{-f^2/(2D_o{}^2)} \quad (2)$$

is applied, where f is the frequency and D_0 is the cutoff frequency of the filter. Taking the inverse Fourier transform returns to the time domain, but with lower frequency components of the signal removed. This allows for the previously described image generation methods to be applied, but with potentially better resolution.

III. Experimental Results

In this section, the focus will be on two different models of SiC transistors referred to in this work as Transistor 1 and Transistor 2. Transistor 1 is shown in the photographs in Fig. 5. These devices generally consist of a ground plane connected to the drain (middle prong), the SiC chip mounted on the drain and wire bonds connecting from the gate and source (outer prongs) to the chip.

International Journal of Emerging Technology and Advanced Engineering
Website: www.ijetae.com (ISSN 2250-2459, ISO 9001:2008 Certified Journal, Volume 4, Issue 1, January 2014)

The challenges with inspecting power transistors are mainly due to the potentially damaging nature of existing inspection methods based on x-ray and SAM as discussed in the Introduction section. Even physical removal of the plastic housing for exact measurement of the device features can be extremely difficult, as the housing must be etched away without destroying some components of the device.

Fig. 6 and Fig. 7 show the THz-TDS c-scan images through the top plastic housing of Transistor 1 and Transistor 2, respectively. These time-domain images are focused on the second reflections from surface S_1 of Fig. 3. All images are taken in the time-domain by returning at each pixel the maximum of the time-domain signal. These show c-scans over the entire plastic housing area of the transistors with scanning step sizes of 150 µm. The results Fig. 6(b, c) and 7(b) show images of higher resolution where the scanning step size is 50 µm. Fig. 6(a, b) and Fig. 7 (a, b) are taken after a Gaussian high-pass filter has been applied to the signal using (2), with D_o = 1.25 THz. For comparison, Fig. 6(b) and Fig. 6(c) illustrate the same data and image generation methods, only Fig. 6(c) does not have the previously described filter applied to the signal.

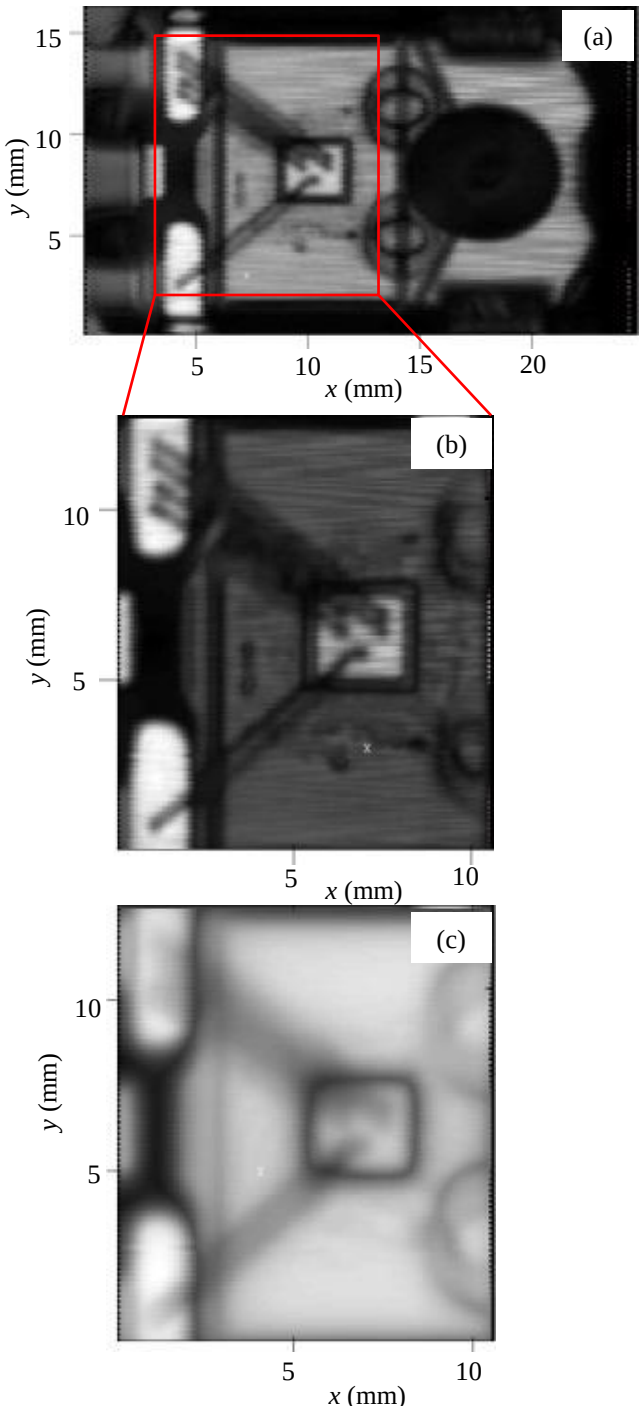

Fig. 6. THz time-domain image through the top surface of Transistor 1. (a) Full area scan with 150 µm^2 pixel size, (b) zoomed scan of SiC chip and wire bonds with 50 µm^2 pixel size and (c) zoomed scan without frequency filter.

International Journal of Emerging Technology and Advanced Engineering
Website: www.ijetae.com (ISSN 2250-2459, ISO 9001:2008 Certified Journal, Volume 4, Issue 1, January 2014)

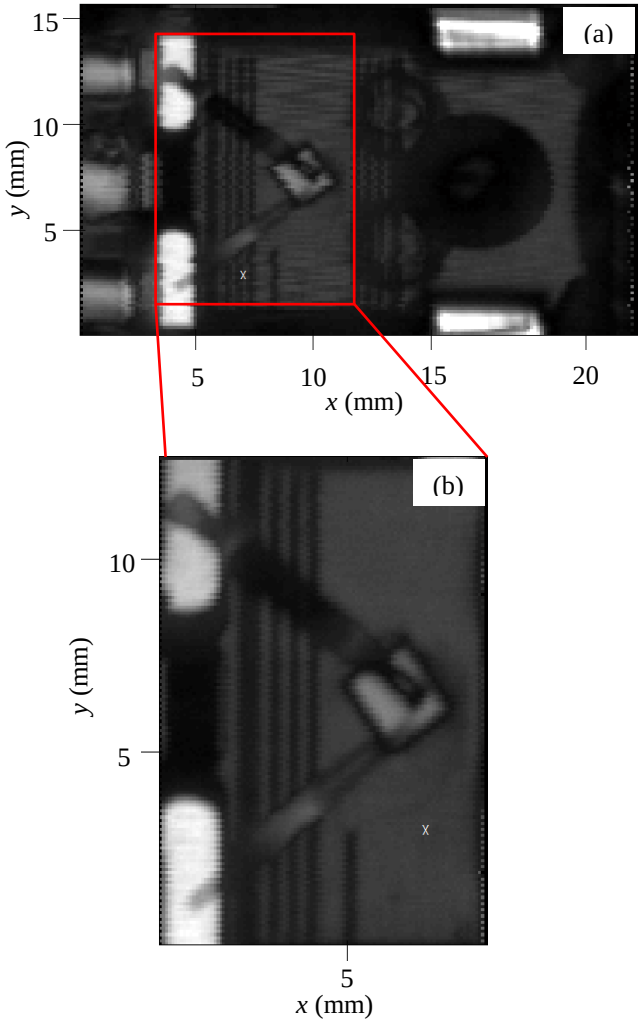

Fig. 7. THz time-domain image through the top surface of Transistor 2 at. (a) Full area scan with 150 μm^2 pixel size and (b) zoomed scan of SiC chip and wire bonds with 50 μm^2 pixel size.

In both Fig. 6 and 7, the three external metal contact prongs of the transistors are visible on the left side of the images (top: source, middle: drain, bottom: gate). The SiC chips are visible at approximately x = -8 mm, y = 1 mm in Fig. 6 and x = -5 mm, y = 0 mm in Fig. 7. The images of Fig. 6 show four wire bonds which are visible connecting the source contact with the SiC chip, each with diameters determined visually to be between 110 μm and 135 μm. The images of Fig. 7 show only a single larger wire bond connecting the source contact to the chip, the diameter being between 410 μm and 560 μm. These dimensions were verified by decapping the devices and taking physical measurements of the wire bonds.

In both transistors only a single wire bond is visible from the gate contact to the SiC chips. The gate of a transistor generally has a much lower electrical current compared to the source and drain. This is why only one wire bond is needed for this contact while more or thicker wires are needed to handle the higher current for the top source contact.

The THz images in both Fig. 6(b) and 7(b) show the gate wire bonds appear to have only single contact points at the SiC chip, but in both images the wire bonds appear to branch out into two separate wires. This lower second wire is not a true feature, but instead a shadow in the image due to the non-normal angle of incidence and reflection of the THz beam. In this THz-TDS system, the incident and reflection angles are 30°. As such, care must be taken when imaging depth-varying features such as this to account for such shadowing effects.

In addition to imaging the packaged device, the height of certain features can be obtained using the time-of-flight depth profiling described in Section II B. In Transistor 1, the distance between the top of the plastic housing and the ground plane at the bottom of the device is measured using a digital micrometer, providing $\Delta h \sim 3.030$ mm. The THz-TDS imaging is used to measure the time difference between the pulses reflected from the top surface of the housing and the ground plane defined as Δt. Equation (1) is used to extract the index of refraction of the housing material n = 1.194. Now that n is known, the height of other features covered by the plastic housing can be calculated. In order to obtain the unknown height of the SiC chip in Fig. 6, the THz beam is focused on locations in Fig. 6 at x = -8 mm, y = 1 mm (on the chip) and x = -8 mm, y = -4 mm (off the chip). The time difference between these reflected pulses, Δt, is then measured. Using equation (1), the height of the chip with respect to the surrounding substrate is then obtained to be 253 μm.

In addition to these SiC transistors, SiC half-bridge modules and high temperature Si solar cells were investigated as well. The half-bridge module was found to have a housing that was too thick for meaningful imaging. The spacing between the top of the housing and nearest feature of interest was greater than 5 mm and multilayered. As such it is expected that attenuation and scattering of the THz beam prevented successful imaging of this device. For the Si solar cells, voiding in the solder connection on the back contact of the device was of interest, however, no such voiding was observed. These devices have 100 nm thick gold (Au) contacts between the Si layer and the solder (where the voiding occurs).

International Journal of Emerging Technology and Advanced Engineering
Website: www.ijetae.com (ISSN 2250-2459, ISO 9001:2008 Certified Journal, Volume 4, Issue 1, January 2014)

Au layers of this thickness do exhibit slight transmission in the THz range, so it was expected that imaging of the voids could be possible [2]. It is likely that the combination of low transmission through the Au layer and absorption in the doped Si layer causes the THz signal to be too attenuated to provide effective imaging of the voids in the solder layer.

IV. Conclusion

THz-TDS reflection imaging was performed for various power electronic devices. For devices encased in a homogenous plastic medium with thicknesses up to several millimeters thick, the system and techniques presented are effective in nondestructively inspecting and profiling the encased features of the devices. For SiC transistors, bond wire number and approximate size were successfully evaluated from c-scan images. Time-of-Flight measurements were implemented to evaluate the refractive index of the housing material and the height of the SiC chip. This indicates that THz imaging could solve issues that usually occur when using common inspection methods such as X-ray, SAM, physical removal of housing, etc. However, the THz-TDS imaging may not be as effective when these devices include thicker housing attenuating layers or metal contacts.

REFERENCES

[1] J Takayanagi et al., "High-Resolution Time-of-Flight Terahertz Tomography using a Femtosecond Fiber Laser," Optics Express, vol. 17, no. 9, pp. 7533-7539, 2009.

[2] N Laman and D Grischkowsky, "Terahertz Conductivity of Thin Metal Films," Appl. Phys. Lett., vol. 93, pp. 051105-1-3, 2008.

[3] P, U Jepsen, R, H Jacobsen, and S, R Keiding, "Generation and Detection of Terahertz Pulses from Biased Semiconductor Antennas," J. Opt. Soc. Am. B, vol. 13, no. 11, pp. 2424-2436, 1996.

[4] M Yamashita et al., "THz Emission Characteristics from p/n Junctions with Metal Lines under Non-bias conditions for LSI Failure Analysis," Optics Express, vol. 19, no. 11, pp. 10864-10873, 2011.

[5] A, J Huber, F Keilmann, J Wittborn, J Aizpurua, and R Hillenbrand, "Terahertz Near-Field Nanoscopy of Mobile Carriers in Single Semiconductor Nanodevices," Nano Lett., vol. 8, no. 11, pp. 3766-3770, 2008.

[6] M Yamashita, Chiko Otani, K Kawase, and K, Tonouchi, M Nikawa, "Noncontact Inspection Technique for Electrical Failures in Semiconductor Devices using a Laser Terahertz Emission Microscope," Appl. Phys. Lett., vol. 93, pp. 041117 1-3, 2008.

[7] B, B Hu and M, C Nuss, "Imaging with Terahertz Waves," Optics Lett., vol. 20, no. 16, pp. 1716-1718, 1995.

[8] L Minkevicius et al., "Detection of Tab Wire Soldering Defects on Silicon Solar Cells using Terahertz Time-Domain Spectroscopy," Electronics Lett., vol. 48, no. 15, 2012.

[9] N Hasegawa, T Loffler, M Thomson, and H Roskos, "Remote Identification of Protrusions and Dents on Surfaces by Terahertz Reflectometry with Spatial Beam Filtering and Out-of-Focus Detection," Appl. Phys. Lett., vol. 83, no. 19, pp. 3996-3998, 2003.

[10] M Tani, S Matsuura, K Sakai, and S Nakashima, "Emission Characteristics of Photoconductive Antennas Based on Low-Temperature-Grown GaAs and Semi-Insulating GaAs," Appl. Optics, vol. 36, no. 30, pp. 7853-7859, 1997.

[11] R, B Silfhout, M, Y Jansen, W, D Driel, and G, Q Zhang, "Designing for 1st and 2nd Level Reliability of Micro-Electronic Packages using Combined Experimental - Numerical Techniques," Proc. IEEE Electron. Comp. and Tech. Conf. , pp. 990-996, 2006.

[12] G Despaux and C De Mello, "High-Frequency Acoustic Imaging with Focused Transducer for Rapid Micro Echography of Interfaces Through Buried Structures Non-Perfectly Planar," in Proc. Acoust. Conf., Nantes, 2012.

[13] J. Kokott, "Power Module Solder-Void Inspection," Inspection Applications, pp. 28-29, Dec. 2011.

[14] K Wada, S Nishizawa, and H Ohashi, "Design and Implementation of a Non-Destructive Test Circuit for SiC-MOSFETs," in Proc. 7th Int. Power Electron. and Motion Control Conf., Harbin, 2012.

[15] W, L Chan, J Deibel, and D, M Mittleman, "Imaging with Terahertz Radiation," Rep. Prog. Phys., vol. 70, pp. 1325-1379, 2007.

[16] H Nakanishi, K Takeya, I Kawayama, H Murakami, and M Tonouchi, "Depth Measurement of Through-Silicon Via Using THz Time-Domain Spectroscopy," in Proc. 36th Int. Conf. IRMMW-THz, Houston, 2011.

[17] C Neubauer, "Intelligent X-Ray Inspection for Quality Control of Solder Joints ," IEEE Trans. Compon. Packag. Manuf. Technol. C, vol. 20, no. 2, pp. 111-120, 1997.